

Characterizing a Cardium waterflood via 3C3D land surface seismic: the Washout Creek experience

Mike Perz*, Xinxiang Li, Mohammad Nemati, Ritesh Kumar Sharma, Satinder Chopra, Peter Cary, and Wendy Ohlhauser, Arcis Seismic Solutions, A TGS Company; Kimberly Pike, Penn West Petroleum Ltd.; and Brian Creaser, Enerplus Corporation

Summary

A high-effort, multicomponent 3C3D seismic data set was acquired over a mature oil field in central Alberta in order to better understand the characteristics of a waterflood operation. True-amplitude processing of the data was undertaken, and joint PP-PS prestack impedance inversion reveals a pronounced set of anomalous low-impedance lineaments at the target level which exhibit a very strong spatial correlation with known water injector locations. Rock physics modeling demonstrates that fluid pressure effects are heavily influencing the seismic response in the vicinity of the injectors, and are accounting for the observed low-impedance anomalies. Analysis of injection and production data suggests that the seismic data can play a vital role in identifying zones of unswept pay in this area.

Introduction

The Washout Creek 3C3D multi-client data set was acquired in west-central Alberta, Canada, in March 2014 (Figure 1). This densely sampled survey was designed to evaluate multiple zones from Cretaceous to Devonian, including the

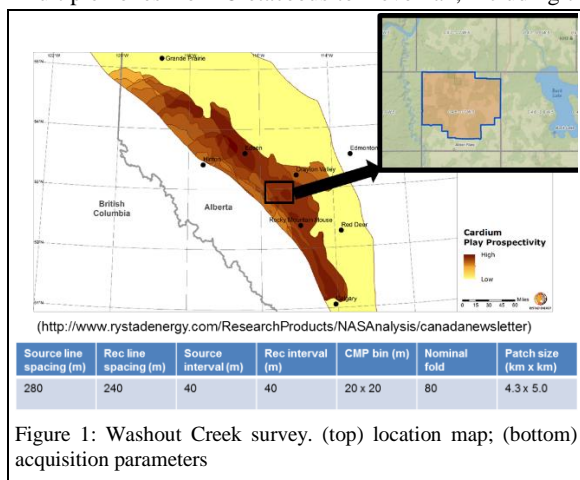


Figure 1: Washout Creek survey. (top) location map; (bottom) acquisition parameters

Duvernay and Cardium formations. The Cardium formation, which constitutes the focus of the present study, contains prolific oil-bearing sandstones whose production in the vicinity of the survey has been bolstered by an extensive waterflooding effort over the past 50 years. The Cardium is quite thin (5-25 m thickness) and in the survey area it contains two distinct units of Late Cretaceous sandstone, both of which lie well below the seismic resolution

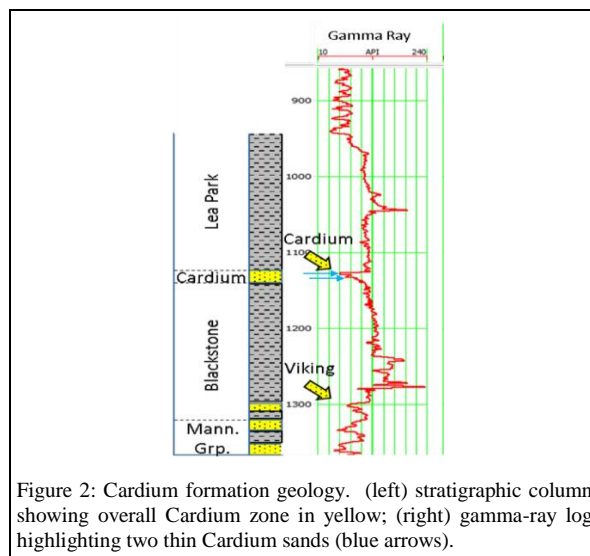


Figure 2: Cardium formation geology. (left) stratigraphic column showing overall Cardium zone in yellow; (right) gamma-ray log highlighting two thin Cardium sands (blue arrows).

threshold. The formation is overlain by the thick Lea Park shale and is underlain by the Blackstone shale (Figure 2).

The main objective behind the survey acquisition was to better understand the waterflood characteristics in order to guide future development. Because core samples at the Cardium level showed a high spatial variability in fracture intensity, it was hoped at the outset of survey planning that wide-azimuth fracture analysis could help characterize the fracture and/or stress regimes; moreover, it was equally anticipated at project inception that elastic parameter inversion would provide valuable information about lithology and fluid variation in the Cardium.

Processing and Inversion Methodology

The data were processed using an azimuthal-AVO-friendly flow which seeks to preserve relative signal amplitude information across both offset and azimuth coordinates. Key steps in the PP processing flow included noise suppression, unbiased surface-consistent scaling (e.g., Nagarajappa and Cary, 2015) and 5D interpolation. Key steps in the PS processing flow included all of the above as well as shear statics corrections and shear-wave-splitting (SWS) compensation. Figure 3 shows amplitude maps at the zone of interest for both a “fast-track” non-AVO-compliant processing flow (top) and the AVO-compliant flow (bottom). Note the strong correlation between low amplitude

Cardium waterflood characterization via 3C3D seismic

lineaments (blue colors) and injector locations on both maps. Within the core of the survey, vertical injectors and producers were generally deployed along a NE-SW “line-drive” pattern whose orientation coincides with the regional direction of maximum horizontal stress (σ_{Hmax}). Although the main benefit of this injector geometry is optimization of sweep efficiency, we note here the serendipitous side-benefit that it facilitates pattern recognition on the seismic maps. It is reassuring to note that the more expensive and rigorous AVO-compliant flow produced a more pronounced anomaly pattern than its non-AVO counterpart.

After processing, the data were input to a myriad of inversion algorithms, including PS and PP azimuthal anisotropy analysis well as joint PP-PS pre-stack impedance inversion.

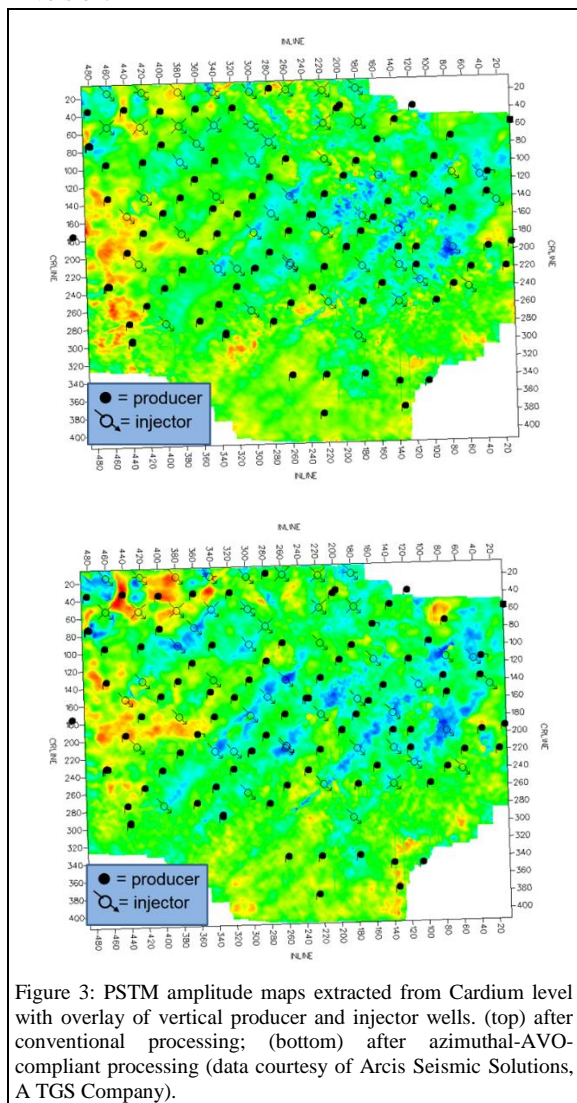


Figure 3: PSTM amplitude maps extracted from Cardium level with overlay of vertical producer and injector wells. (top) after conventional processing; (bottom) after azimuthal-AVO-compliant processing (data courtesy of Arcis Seismic Solutions, A TGS Company).

Discussion of Results

In this section we discuss our key observations and relate them to well control. Although several horizontal and deviated wells are present throughout the survey, they have been excluded from our analysis due to uncertainty in locating their effective production and injection contributions along the lateral wellbores. Thus we are considering only point data from vertical wells in the present work.

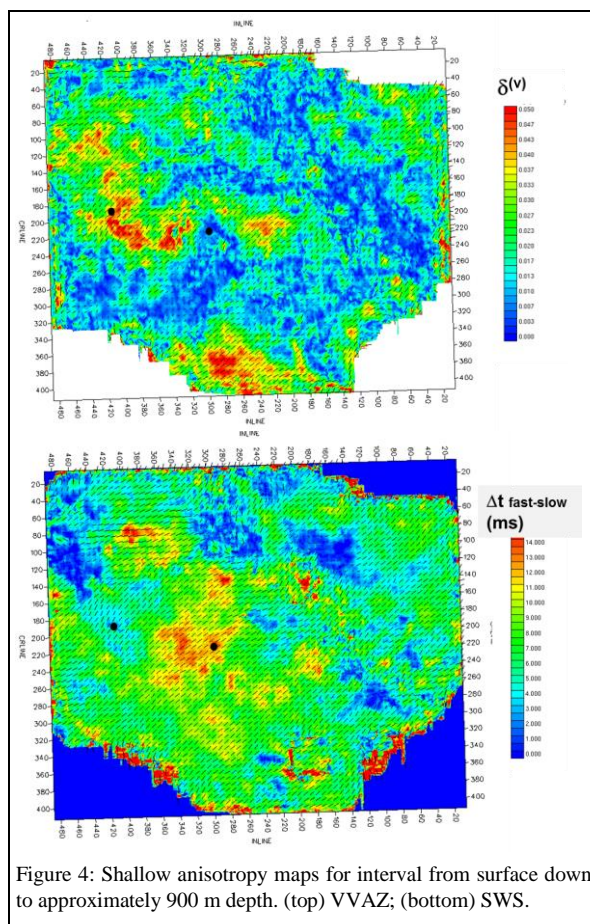


Figure 4: Shallow anisotropy maps for interval from surface down to approximately 900 m depth. (top) VVAZ; (bottom) SWS.

Fracture attributes

Figure 4 shows anisotropy maps generated from both PP azimuthal velocity inversion (VVAZ) and PS SWS analysis. In each case the analysis window was chosen to characterize the anisotropy of the shallow overburden. Note that both maps show the expected NE-SW orientation trend, consistent with the direction of expected regional σ_{Hmax} in the area, and also consistent with results from a nearby microseismic program. Despite this similarity in orientation, intensity patterns show significant differences. It is possible

Cardium waterflood characterization via 3C3D seismic

that this discrepancy is related to spatial variations in the type of fluid filling the aligned fractures (M. Chapman, personal communication, 2015). This hypothesis is supported by the physical modeling work of Tillotson et al. (2014) who observed that the Thomsen parameter δ (which controls the VVAZ response) changed dramatically in their fractured sandstone samples depending on the type of fluid fill, while the Thomsen parameter γ (which controls the shear-wave-splitting) did not. Although not shown here, the corresponding deeper-layer fracture maps suggest that a laterally and vertically homogeneous orientation field exists from surface down to an appreciable depth below the Cardium level. This interpretation has somewhat allayed initial concerns that strong localized overburden fracturing might be significantly influencing the waterflood.

Inversion attributes

Figure 5 shows P-impedance maps produced by pre-stack inversion using two different approaches. In the first scheme (Figure 5, top) the PP data alone were inverted, while in the second (Figure 5, bottom) both PP and PS data were combined in a joint inversion. The marked improvement in correlation between low-impedance lineaments and injector locations after joint PP-PS inversion suggests that the added information provided by the PS data is improving inversion reliability.

Production/injection data analysis

Figure 6 shows an overlay of production and injection data atop a greyscale version of the P-impedance map from joint PP-PS inversion (i.e., same map as in Figure 5, bottom). In order to avoid the potentially confusing effects associated with (i) well-to-well variability in the duration of production/injection and (ii) the shutdown of certain wells over the lifetime of this prolonged waterflood, we chose to consider only those production/injection data associated with the 24 month period preceding survey acquisition. The figure suggests that regions of strong pressure support (inferred to be areas adjacent to the large injection bubbles) correspond to low impedance values. While other correlations between well information and seismic data seem to exist on this map (e.g., high impedance values in the south correlate with low production and a lack of injection), it is important to recognize that analysis is complicated by the fact that the long-wavelength spatial variation in impedance is influenced by known regional variations in lithology.

Rock Physics Modeling

Our intriguing observation of correlation between low P-impedance values and high water injection volumes was further investigated using rock physics modeling. In an effort to better understand how changes in pore fluids affect the seismic response, Gassmann fluid replacement modeling

was applied to a type well for the Cardium. This simplistic modeling approach assumes that the load-induced pore pressure is homogeneous and identical in all pores (Berryman, 1999). V_p , V_s , density, lambda-rho and mu-rho model well logs were predicted using appropriate reservoir parameters for both injector (water-filled pore space) and producer (oil-filled pore space) scenarios and results are shown in Figure 7 (top). Note that there is minimal variation in V_p and V_s with fluid type, while density (and, by inference, P-impedance) decreases in the producer case (red curve) and increases in the injector (blue curve) case.

Because this modeled seismic response did not support our observation of low impedance values at injector wells, a more sophisticated modeling approach was adopted which considers the effect of pore pressure changes. The pore pressure effect was modeled using the technique of MacBeth

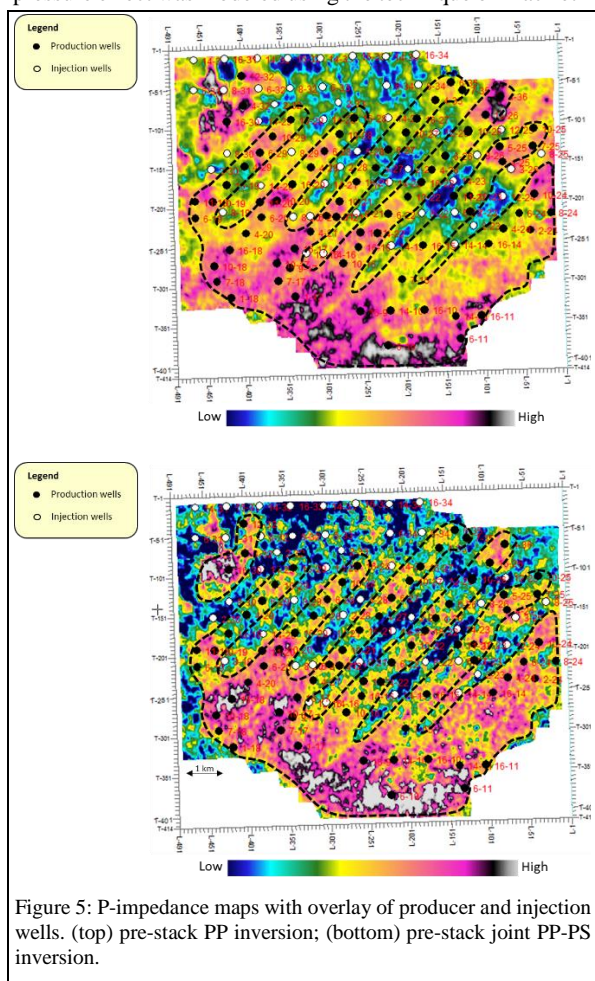


Figure 5: P-impedance maps with overlay of producer and injection wells. (top) pre-stack PP inversion; (bottom) pre-stack joint PP-PS inversion.

(2004), and the fluid substitution effect was again modeled using Gassmann. At injectors the pore pressure was increased by 15 MPa, and the pore spaces were filled with

Cardium waterflood characterization via 3C3D seismic

water; at producers the pore pressure was drawn down by 15 MPa, and the pore spaces filled with oil. In addition, a small amount of gas was introduced to the pore space at producers to account for the dissolution of gas from oil below the bubble point.

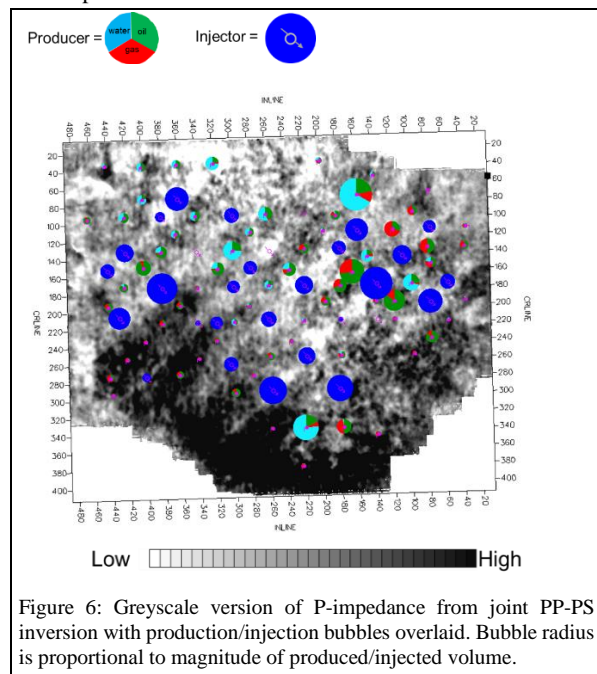


Figure 6: Greyscale version of P-impedance from joint PP-PS inversion with production/injection bubbles overlaid. Bubble radius is proportional to magnitude of produced/injected volume.

The results of the MacBeth-Gassmann modeling are shown in Figure 7 (bottom). The modeled response is significantly different from that observed using Gassmann alone. In particular the density shows minimal change under either production/injection scenarios, while both V_s and V_p (and, by inference, P-impedance) show a decrease at injectors and an increase at producers, in harmony with our observations. Thus by simultaneously accounting for both pore pressure and fluid substitution effects, we have successfully predicted our real-world observation of low impedance values corresponding to injector wells locations. It is interesting to note that Calvert et al., (2014) undertook a similar study in a North Sea carbonate waterflood, but in their case the fluid substitution effect tended to dominate, and they observed an increase, rather than a decrease, in P-impedance at injectors.

Conclusions

Low P-impedance anomalies observed on maps generated from the seismic data show a strong correlation with injector well locations. The degree of correlation improves with the use of careful AVO-compliant processing and also with the inclusion of PS data in a joint PP-PS inversion. Rock physics

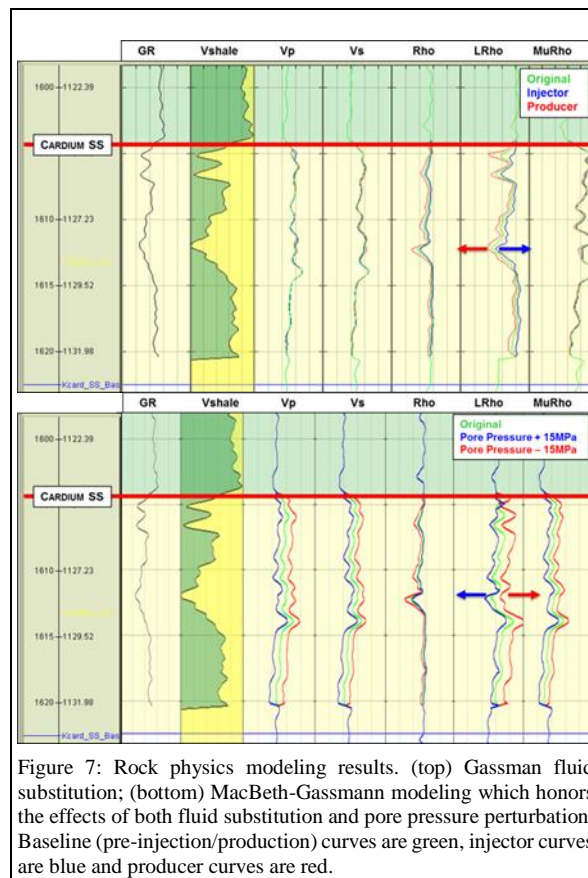


Figure 7: Rock physics modeling results. (top) Gassman fluid substitution; (bottom) MacBeth-Gassmann modeling which honors the effects of both fluid substitution and pore pressure perturbation. Baseline (pre-injection/production) curves are green, injector curves are blue and producer curves are red.

modeling predicts a lowering of impedance at injector site locations, consistent with our observations. PP and PS anisotropy analysis reveals an essentially uniform overburden orientation field, consistent with the regional direction of maximum horizontal stress. Although further work is required to better understand the complex relationship between the seismic-derived elastic attributes, zones of good/poor production and zones of high/low volume of water injection, the current work strongly suggests that 3C3D seismic data should play an important role in optimizing future Cardium waterflood operations.

Acknowledgements

We thank Mark Chapman (Edinburgh Anisotropy Project) and Henrik Roende (TGS) for helpful discussions. We thank Jeremy Gallop (Ikon Science) for performing the rock physics modelling and Fuchang Guo (Arcis) for his programming efforts. We acknowledge Enerplus Corporation and Arcis Seismic Solutions for granting permission to publish this work.

EDITED REFERENCES

Note: This reference list is a copyedited version of the reference list submitted by the author. Reference lists for the 2016 SEG Technical Program Expanded Abstracts have been copyedited so that references provided with the online metadata for each paper will achieve a high degree of linking to cited sources that appear on the Web.

REFERENCES

- Berryman, J. G., 1999, Origin of Gassman's equations: *Geophysics*, **64**, 1627–1629, <http://dx.doi.org/10.1190/1.1444667>.
- Calvert, M. A., L. D. Vagg, K. B. Lafond, A. R. Hoover, K. C. Ooi, and I. H. Herbert, 2014, Insights into sweep efficiency using 4D seismic at Halfdan field in the North Sea: *The Leading Edge*, **33**, 182–187, <http://dx.doi.org/10.1190/tle33020182.1>.
- MacBeth, C., 2004, A classification for the pressure-sensitivity properties of a sandstone rock frame: *Geophysics*, **69**, 497–510, <http://dx.doi.org/10.1190/1.1707070>.
- Nagarajappa, N., and P. W. Cary, 2015, Unbiased surface-consistent scalar estimation by crosscorrelation: 85th Annual International Meeting, SEG, Expanded Abstracts, 2337–2341, <http://dx.doi.org/10.1190/segam2015-5909720.1>.
- Tillotson, P., M. Chapman, J. Sothcott, A. I. Best, and X. Li, 2014, Pore fluid viscosity effects on P- and S-wave anisotropy in synthetic silica-cemented sandstone with aligned fractures: *Geophysical Prospecting*, **62**, 1238–1252, <http://dx.doi.org/10.1111/1365-2478.12194>.